4. K. Briffa *et al.*, *Nature* **393**, 350 (1998).
5. P. Jones *et al.*, *Holocene* **8**, 455 (1998).
6. M. E. Mann, R. S. Bradley, M. K. Hughes, *Geophys. Res. Lett.* **26**, 759 (1999).
7. T. J. Crowley, *Science* **289**, 270 (2000).
8. C. Pfister, in *Climate Since A.D. 1500*, R. S. Bradley, P. D. Jones, Eds. (Routledge, London, 1995), pp. 118–142.
9. D. T. Shindell, D. Rind, N. Balachandran, J. Lean, P. Lonergan, *Science* **284**, 305 (1999).
10. D. T. Shindell, D. Rind, P. Lonergan, *J. Clim.* **11**, 895 (1998).
11. D. J. Wuebbles, C.-F. Wei, K. O. Patten, *Geophys. Res. Lett.* **25**, 523 (1998).
12. Because 2D photochemical models have difficulty accounting for the dynamically driven stratospheric hydrological cycle, we prescribed stratospheric water vapor changes due to methane oxidation by conserving hydrogen in ($2 \times CH_4 + H_2O$), which satellite data show is roughly constant. Long-term methane trends were taken from ice core data, which show approximately 60% less methane during the preindustrial period. Observations from the Halogen Occultation Experiment instrument, version 18 data, obtained from the NASA Langley data center, were used to determine the fraction of methane oxidized throughout the stratosphere. For example, at 1 mbar in mid-latitudes, ~1.6 parts per million by volume (ppmv) of water was removed relative to the present based on 80% oxidation of the 1.0-ppmv methane change. This assumes that the preindustrial methane oxidation rate in the stratosphere was as large as that at present. This is fundamental to the negative ozone response, which differs from that seen in a previous study (*11*).
13. Ozone's temperature sensitivity is governed by catalytic cycles involving chlorine, nitrogen, hydrogen, and oxygen radicals. The temperature dependence of the rate-limiting reactions for the chlorine, nitrogen, and hydrogen cycles is weakly negative, whereas for oxygen it is strongly positive. The relative importance of the oxygen cycle was greater during the preindustrial period, leading to large increases in overall temperature sensitivity in the upper stratosphere.
14. J. Hansen, M. Sato, R. Ruedy, *J. Geophys. Res.* **102**, 6831 (1997).
15. D. V. Hoyt, K. H. Schatten, *J. Geophys. Res.* **98**, 18,895 (1993).
16. D. W. J. Thompson, J. M. Wallace, *Geophys. Res. Lett.* **25**, 1297 (1998).
17. J. M. Wallace, *Quart. J. R. Meterol. Soc.* **126**, 791 (2000).
18. V. C. Slonosky, P. D. Jones, T. D. Davies, *Int. J. Climatol.* **21**, 285 (2001).
19. M. E. Mann, R. S. Bradley, M. K. Hughes, *Nature* **392**, 779 (1998).
20. Because the pattern reconstructions are smoothed by retaining only a truncated eigenvector basis set, the amplitude of regional temperature variations is generally underestimated. This is particularly true before 1730, when five or fewer eigenvectors are retained.
21. A. M. Waple, M. E. Mann, R. S. Bradley, *Clim. Dyn.*, in press.
22. D. T. Shindell, G. A. Schmidt, R. L. Miller, D. Rind, *J. Geophys. Res.* **106**, 7193 (2001).
23. L. D. Keigwin, R. S. Pickart, *Science* **286**, 520 (1999).
24. P. Bergthórsson, *Jàkull* **19**, 94 (1969).
25. D. T. Shindell, R. L. Miller, G. A. Schmidt, L. Pandolfo, *Nature* **399**, 452 (1999).
26. For forcing by greenhouse gases, the enhanced latitudinal gradient is further strengthened by their cooling effect in the stratosphere. Ozone depletion and volcanic forcing enhance the AO by an abbreviated mechanism, directly altering temperatures near the tropopause as in step (iii).
27. Y. Ohhashi, K. Yamazaki, *J. Meteorol. Soc. Jpn.* **77**, 495 (1999).
28. D. L. Hartmann, J. M. Wallace, V. Limpasuvan, D. W. J. Thompson, J. R. Holton, *Proc. Natl. Acad. Sci. U.S.A.* **97**, 1412 (2000).
29. The flux changes are roughly –1/3 those seen in our greenhouse gas forcing simulations (*22*, *25*), which is consistent with the AO response ratio.
30. Temperature change was calculated as the difference between simulations, using 1900 and 1990s irradiance, both with 1990s atmospheric composition. However, the influence of irradiance changes cannot be fully separated from that of the changing atmospheric composition on ozone photochemistry or the nonlinear long-term dynamical and chemical responses.
31. G. C. Hegerl *et al.*, *Clim. Dyn.* **13**, 613 (1997).
32. N. Gillett *et al.*, *J. Geophys. Res.*, in press.
33. U. Cubasch *et al.*, *Clim. Dyn.* **13**, 757 (1997).
34. B. Rajagopalan, Y. Kushnir, Y. M. Tourre, *Geophys. Res. Lett.* **25**, 3967 (1998).
35. M. P. Hoerling, J. W. Hurrell, T. Xu, *Science* **292**, 90 (2001).
36. M. Free, A. Robock, *J. Geophys. Res.* **104**, 19,057 (1999).
37. T. L. Delworth, K. W. Dixon, *J. Clim.* **13**, 3721 (2000).
38. W. S. Broecker, *Proc. Natl. Acad. Sci U.S.A.* **97**, 1339 (2000).
39. M. Visbeck, H. Cullen, G. Krahmann, N. Naik, *Geophys. Res. Lett.* **25**, 4521 (1998).
40. Supplemental Web material is available on *Science* Online at www.sciencemag.org/cgi/content/full/294/5549/2149/DC1.
41. Stratospheric climate modeling at GISS is supported by NASA's Atmospheric Chemistry Modeling and Analysis Program. G.A.S. and D.T.S. acknowledge the support of NSF grant ATM-00-02267. M.E.M. acknowledges support from the National Oceanic and Atmospheric Administration– and NSF-supported Earth Systems History program. We thank J. Lean for providing the solar irradiance reconstruction.

13 July 2001; accepted 31 October 2001

Glacial-to-Holocene Redistribution of Carbonate Ion in the Deep Sea

Wallace S. Broecker* and Elizabeth Clark

We have reconstructed the glacial-age distribution of carbonate ion concentration in the deep waters of the equatorial ocean on the basis of differences in weight between glacial and Holocene foraminifera shells picked from a series of cores spanning a range of water depth on the western Atlantic's Ceara Rise and the western Pacific's Ontong Java Plateau. The results suggest that unlike today's ocean, sizable vertical gradients in the carbonate ion concentration existed in the glacial-age deep ocean. In the equatorial Pacific, the concentration increased with depth, and in the Atlantic, it decreased with depth. In addition, the contrast between the carbonate ion concentration in deep waters produced in the northern Atlantic and deep water in the Pacific appears to have been larger than in today's ocean.

Chemical feedbacks operating in the ocean lead to adjustments in its carbonate ion (CO_3^{2-}) concentration which ensure that the burial of calcite and aragonite formed by marine organisms does not exceed the supply to the ocean of the ingredients required for the manufacture of these minerals (i.e., CO_2 and CaO) (*1*, *2*). In today's ocean the large overproduction of $CaCO_3$ hardparts by marine organisms is compensated by dissolution. The CO_3^{2-} concentration is driven to that level where the excess production (over supply) is redissolved. Because the solubility of calcite increases with pressure (*3–5*), the tendency to dissolve intensifies with depth. Consequently, the "red clays" that coat the ocean's abyssal plains have lost all their $CaCO_3$ to dissolution. By contrast, the "oozes" that drape the ocean's ridge crests and plateaus are rich in $CaCO_3$. A transition zone characterized by decreasing $CaCO_3$ content separates the realm of preservation from that of complete dissolution.

Although through much of the deep sea the CO_3^{2-} concentration is quite uniform (84 ± 3 μmol/kg), that part of the deep Atlantic occupied by North Atlantic Deep Water (NADW) has a significantly higher concentration of this ion (i.e., 112 ± 4 μmol/kg) (*6*). The higher CO_3^{2-} concentration in NADW leads to a deeper transition zone in the Atlantic than in the Pacific Ocean.

Since 1970, many studies have been carried out to determine how the transition-zone depth differed during glacial time (*7–17*). The consensus from these studies is that it was shallower in the Atlantic and deeper in the Pacific. However, the methods used to reconstruct these changes are either qualitative or subject to multiple interpretations. We have adopted the method described by Lohmann (*18*, *19*) to reconstruct the distribution of CO_3^{2-} in the glacial deep sea by weighing shells of a given planktonic species picked from a fixed size range. This approach is based on the observation that shells lose on the average about 1% of their mass for each μmol/kg decrease in the pressure-normalized bottom-water CO_3^{2-} concentration [$CO_3^{2-*} = CO_3^{2-} + 20(4 - z)$, where z is the water depth (in km) and the units for CO_3^{2-} concentration are μmol/ kg (*20*)].

For this study, we selected cores from a

Lamont-Doherty Earth Observatory of Columbia University, Palisades, NY 10964, USA.

*To whom correspondence should be addressed. E-mail: broecker@ldeo.columbia.edu

series of water depths on the Ceara Rise in the western equatorial Atlantic and on the Ontong Java Plateau in the western equatorial Pacific. We made shell-weight measurements on three planktonic species: *Globigerinoides sacculifer*, *Pulleniatina obliquiloculata*, and *Neogloboquadrina dutertrei* (50 shells each) picked from the 355- to 420-μm-size fraction. The results are summarized in Web table 1 (*21*) and Fig. 1. We adopted a 0.3-μg drop in shell weight per μmol/kg drop in pressure-normalized CO_3^{2-} concentration (*20*) to convert shell-weight differences to CO_3^{2-} concentration changes. As summarized in Fig. 2, these results suggest that the CO_3^{2-} gradient in the glacial deep Atlantic was far steeper than it is today. At 2800-m depth, the CO_3^{2-} concentration appears to have been about 28 μmol/kg higher than in today's ocean, and at 4.0 km it appears to have been as much as 23 μmol/kg lower than in today's ocean. The depth separating waters with higher from those with lower concentrations was about 3.5 km. In the Pacific, little glacial-to-Holocene change in CO_3^{2-} concentration occurred at 2.3-km depth, but at 4.0 km, the CO_3^{2-} concentration was about 18 μmol/kg higher during glacial time than it is now. The uncertainty for a given shell-weight measurement is on the order of 2 μg. When expressed as CO_3^{2-} concentration, 2 μg corresponds to 7 μmol/kg (*22*).

Attempts to reconstruct past CO_3^{2-} distributions suffer from the common drawback that much of the dissolution occurs in the sediment pore waters rather than on the sea floor (*23–28*). This dissolution is driven by respiration CO_2, which lowers the pore-water CO_3^{2-} concentration below that in bottom water, thereby permitting dissolution to occur well above the calcite saturation horizon (i.e., that level separating the overlying waters supersaturated with calcite from the underlying waters undersaturated with calcite). Because of this complication, our shell-weight measurements record CO_3^{2-} concentration changes in the pore water rather than bottom water. They can be applied to bottom water only with the assumption that the offset between the CO_3^{2-} concentration in bottom water and pore water was the same during glacial time as it is today. Because the magnitude of this offset depends on the rain rate of organic material to the sea floor, it is subject to change.

The method described by Lohmann (*18*, *19*) also depends on the assumption that initial shell calcite thickness does not undergo changes with growth environment. We have shown that at least for *P. obliquiloculata* and *N. dutertrei*, this is not the case (*20*). Rather, the initial thickness varies with growth locale. Therefore, we studied cores from a range of water depths at the same locale so that at any given time the shells were supplied from the same surface-water source. Hence, differential weight changes from depth to depth cannot be attributed to variable growth conditions. But the only way in which shell weights for Atlantic and Pacific samples of the same age or in which Holocene and glacial samples from the same place can be tested to ascertain the influence of differences in initial shell thickness is to examine the concordance among species, the assumption being that changes in growth conditions should not impact all species by the same amount.

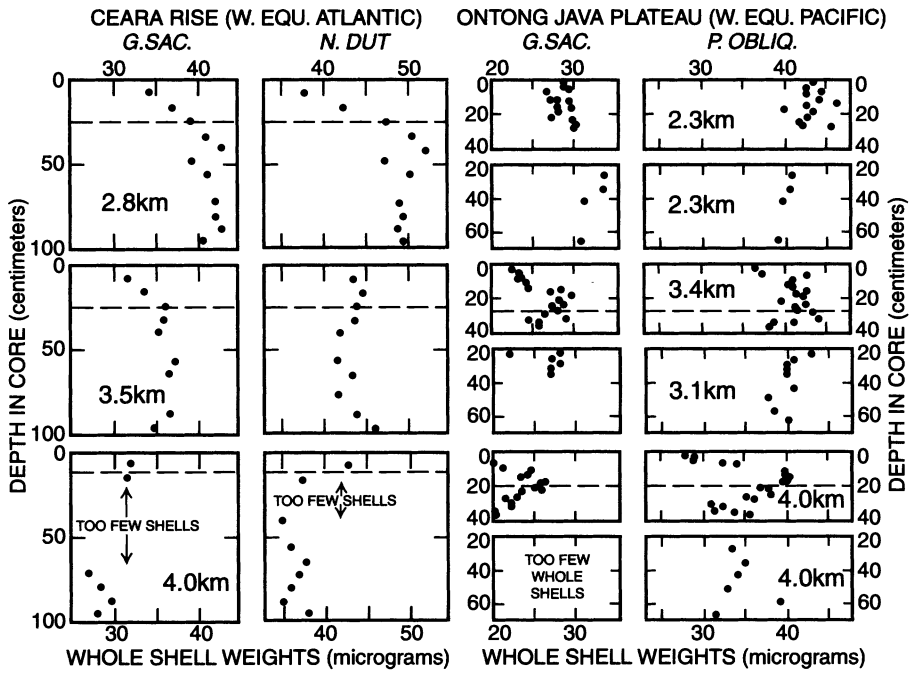

Fig. 1. Plots of average whole-shell weights as a function of depth in the sediment cores. **(Left)** Results of three giant gravity cores from the Atlantic's Ceara Rise (5°N). (Top to bottom: KNR110-82, KNR110-66, and KNR110-50.) The dashed lines mark the midpoint of the glacial-to-Holocene large increase in $CaCO_3$ content (*36*, *37*). The sections in the deepest core where too few whole shells were present represent zones of sufficiently intense dissolution to lead to shell disintegration. **(Right)** Results from six equatorial cores from the Pacific's Ontong Java Plateau. (Top to bottom: MW91-9-36, MW91-9-15, MW91-9-51, V28-238, MW91-9-56, and MW91-9-55.) Three of these (the top of each depth-pair) are box cores on which detailed sampling was conducted, allowing the decline in shell weight following the Termination I preservation event (*36*, *37*) to be documented. The other three (the bottom of each depth-pair) are piston or giant gravity cores that penetrated into glacial-age sediment. For these cores, only measurements on samples from below Termination I are plotted. The box cores were ^{14}C-dated (*37*). The dashed line marks the depth at which the ^{14}C age is 13,000 years. The position of the midpoint of the Termination I in the longer cores is based on ^{18}O measurements on planktonic foraminifera. In the deepest pair of cores, whole *G. sacculifer* shells were present only in the section representing the Termination I preservation event.

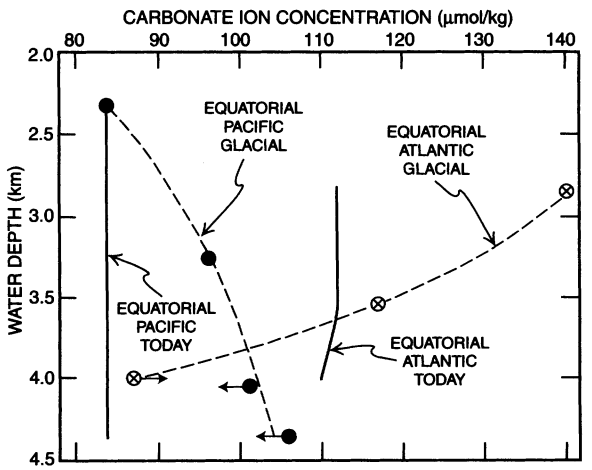

Fig. 2. Reconstruction of the CO_3^{2-} concentration in the equatorial zones of the glacial Atlantic and Pacific. The reconstruction is based on the weight differences between core-top and glacial-age whole foraminifera shells [Web table 1 (*21*)]. The glacial–to–late Holocene CO_3^{2-} differences are calculated on the basis of the 0.3 μg per μmol per kg relation (*20*). These differences are referenced to the global CO_3^{2-} distribution established by measurements made as part of the GEOSECS survey. The arrows indicate the direction of change in the case of doglegs in the relation between shell weight and pressure-normalized CO_3^{2-} concentration.

The relation between shell weight and pressure-normalized CO_3^{2-} concentration likely terminates in a dogleg, because at the depth of the saturation horizon, a second mechanism for dissolution comes into play, namely, dissolution while the shell lies on the sea floor. This weight loss would have to be added to that which occurs in the pore water, thus steepening the weight-loss dependence on pressure-normalized CO_3^{2-} concentration. Our deepest Pacific cores are likely currently bathed in waters undersaturated with respect to calcite.

Finally, as the pressure-normalized CO_3^{2-} concentration increases, it would be expected that a point would be reached where the excess CO_3^{2-} content of bottom water would no longer be able to compensate for reduction in the pore waters caused by the release of respiration CO_2. If so, one would expect an up-water-column decrease in the coefficient relating shell-weight loss to pressure-normalized CO_3^{2-} concentration.

The results presented here are consistent with the traditional concept that the lysocline in the Pacific was deeper during glacial time, whereas that in the Atlantic was shallower (*7–17*). But this shift in the Atlantic lysocline is not the result of a lower CO_3^{2-} concentration in NADW (it was higher during glacial time). Rather, it is more likely due to an upward shift in the interface separating low–CO_3^{2-} content Antarctic Bottom Water (AABW) from high–CO_3^{2-} content NADW. In today's ocean, AABW has a CO_3^{2-}concentration that is 30 μmol/kg lower than that of NADW; hence, if AABW were to displace NADW, there would be a 1.5-km shoaling of the lysocline.

It is tempting to attribute the high glacial CO_3^{2-} concentration at 2.8-km depth in the tropical Atlantic to the presence of low-nutrient upper glacial NADW. But, as shown by cadmium (*29*) and barium (*30*, *31*) measurements on benthic foraminifera, the transition between glacial-age upper and lower NADW was considerably shallower (i.e., at about 2.3-km depth).

Although it might be expected that CO_3^{2-} concentration would be inversely related to nutrient concentration, the situation is not so simple. The complication has to do with the transport of CO_2 through the atmosphere and with sea-floor $CaCO_3$ dissolution. If the ocean were a closed system with respect to communication with the atmosphere and its sediments, one would indeed expect an inverse relation between nutrient concentration and CO_3^{2-} concentration; the respiration CO_2 associated with the nutrients would remain in the water and react with CO_3^{2-} (and HBO_3^-) and hence drive down the CO_3^{2-} concentration. In today's ocean, deep water forming in the Southern Ocean has about 0.8 μmol/kg more PO_4 than that forming in the northern Atlantic. On the basis of an O_2-to-PO_4 Redfield coefficient of 125 (*32*), this difference corresponds to 100 μmol/kg of respiration CO_2. If the ocean were a closed system, newly formed Southern Ocean deep water should have a CO_3^{2-} concentration of about 85 μmol/kg less than that in newly formed northern Atlantic deep water. But the observed difference between the CO_3^{2-} concentrations in these end-member water types is only about 30 μmol/kg (*6*), mainly because CO_2 moves through the atmosphere. As shown by Broecker and Peng (*33*), this leads to a release of CO_2 from high-nutrient Southern Ocean surface waters and an uptake of CO_2 by northern Atlantic surface waters. The impact of this transfer is to reduce the difference between the respiration CO_2 burdens of these two water types and hence also in their initial CO_3^{2-} concentrations. So when considering the glacial contrast, it is not only the difference in nutrient concentration that has to be considered but also the efficiency with which CO_2 transport took place through the atmosphere. In today's ocean, the impact of this transfer is large.

A puzzling aspect of our reconstruction is that the CO_3^{2-} concentration at 4-km-depth water in the Atlantic appears to have been reduced to lower CO_3^{2-} concentration than that for 4-km-depth water in the equatorial Pacific. If this reconstruction proves to be correct, then the pattern of thermohaline circulation during glacial time must have been fundamentally different than it is today. But, as already mentioned, if a dogleg exists in the relation between weight loss and pressure-corrected CO_3^{2-} concentration, then the changes in CO_3^{2-} concentration at 4-km depth may be smaller than shown in Fig. 2, and the CO_3^{2-} concentrations at 4-km depth in the two oceans may have been similar.

Also puzzling is that the large vertical gradient in the Atlantic's CO_3^{2-} concentration is not seen in either the benthic ^{13}C (*34*) or ^{14}C (*35*) results. As summarized in Web table 2 (*21*), the $\delta^{13}C$ values for glacial benthic foraminifera were nearly identical ($+0.3 \pm 0.1$‰) for the depths of the three cores studied here. Also summarized in Web table 2 (*21*) are the differences between the ^{14}C ages for glacial-age benthic and planktonic foraminifera from these same three Ceara Rise cores (*35*). Again, no significant difference exists. Neither the ^{13}C nor the ^{14}C results are consistent with the interpretation that the penetration of Southern Ocean waters into the deep Atlantic was more pronounced at 4.0-km than at 3.5-km depth. If so, one would expect even lower benthic ^{13}C to ^{12}C and ^{14}C to C ratios.

Of course, one could attribute these gradients to changes in pore-water rather than bottom-water CO_3^{2-} concentrations. This would require that during glacial time a substantially smaller fraction of the organic debris falling from the surface Pacific reached 4 km and that a substantially larger fraction reached that depth in the Atlantic. Moreover, not only may the offset between bottom-water and pore-water CO_3^{2-} concentration have differed during glacial time, but these differences may also have varied regionally. Changes in initial shell thickness and the existence of doglegs in the shell weight versus pressure-normalized CO_3^{2-} concentration may further complicate the situation.

Whatever the explanation, the large gradients in CO_3^{2-} concentration in the glacial ocean have important implications because, with one exception, such gradients are absent in today's ocean. The exception is the western basin of the South Atlantic where low–CO_3^{2-} concentration AABW underrides high–CO_3^{2-} NADW. In the narrow transition zone between these water masses, a steep gradient exists. But elsewhere in the present-day deep ocean, there is virtually no gradient with depth in CO_3^{2-} concentration. Thus, our results suggest that the waters supplying the deep sea had a greater range in density, thereby permitting stratification to persist.

References and Notes

1. W. S. Broecker, in *The Late Cenozoic Glacial Ages*, K. K. Turekian, Ed. (Yale Univ. Press, New Haven, CT, 1971).
2. ———, *Quat. Res.* **1**, 188 (1971).
3. R. M. Pytkowicz, G. A. Fowler, *Geochem. J.* **6**, 169 (1967).
4. F. J. Millero, R. A. Berner, *Geochim. Cosmochim. Acta* **36**, 92 (1972).
5. F. L. Sayles, *Mar. Chem.* **9**, 223 (1980).
6. W. S. Broecker, S. Sutherland, *G*^{3} 1 GC000039 (2000).
7. G. R. Heath, C. Culberson, *Geol. Soc. Am. Bull.* **81**, 3157 (1970).
8. T. J. Crowley, *Mar. Geol.* **51**, 1 (1983).
9. L. C. Peterson, W. L. Prell, in *Geophysical Monograph 32, The Carbon Cycle and Atmospheric CO_2: Natural Variations Archean to Present*, E. T. Sundquist, W. S. Broecker, Eds. (American Geophysical Union, Washington, DC, 1985), pp. 251–269.
10. W. B. Curry, G. P. Lohmann, in *Geophysical Monograph 32, The Carbon Cycle and Atmospheric CO_2: Natural Variations Archean to Present*, E. T. Sundquist, W. S. Broecker, Eds. (American Geophysical Union, Washington DC, 1985), pp. 285–301.
11. J. W. Farrell, W. L. Prell, *Paleoceanography* **4**, 447 (1989).
12. G. Wu, M. K. Yasuda, W. H. Berger, *Mar. Geol.* **99**, 135 (1991).
13. J. W. Farrell, W. L. Prell, *Paleoceanography* **6**, 485 (1991).
14. R. Karlin, M. Lyle, R. Zahn, *Paleoceanography* **7**, 43 (1992).
15. J. Le, N. J. Shackleton, *Paleoceanography* **7**, 21 (1992).
16. W. R. Howard, W. L. Prell, *Paleoceanography* **9**, 453 (1994).
17. M. P. Stephens, D. C. Kadko, *Paleoceanography* **12**, 797 (1997).
18. G. P. Lohmann, *Paleoceanography* **10**, 445 (1995).
19. The Lohmann method involves thorough cleaning and sonification of the greater than 63-μm-size fraction followed by the isolation of the 355- to 425-μm-size fraction from which are picked about 50 whole foraminifera shells of a given planktonic species. These shells are weighed as a group on a microbalance, and the average shell weight is calculated.
20. W. S. Broecker, E. Clark, *Paleoceanography* **16**, 531 (2001).

21. Supplementary Web material is available on *Science* Online at www.sciencemag.org/cgi/content/full/294/5549/2152/DC1.
22. A blind intercomparison study conducted with Lohmann revealed that after normalization for a 2.4-μg average difference between his weight measurements and ours, the mean difference between his measurements and ours was about 2 μg. The range of individual shell weights suggests that if 50 shells are weighed, there is a statistical uncertainty of between 1 and 2 μg resulting from the finite number of shells weighed. Finally, 15 Holocene samples from a core at 2.3-km depth on the Ontong Java Plateau yielded a mean deviation of 1.5 μg.
23. D. Archer, S. Emerson, C. Reimers, *Geochim. Cosmochim. Acta* **53**, 2831 (1989).
24. S. R. Emerson, D. Archer, *Philos. Trans. R. Soc. London Ser. A* **331**, 29 (1990).
25. B. Hales, S. Emerson, D. Archer, *Deep-Sea Res. I* **41**, 695 (1994).
26. B. Hales, S. Emerson, *Global Biogeochem. Cycles* **10**, 527 (1996).
27. W. R. Martin, F. L. Sayles, *Geochim. Cosmochim. Acta* **60**, 243 (1996).
28. B. Hales, S. Emerson, *Geochim. Cosmochim. Acta* **61**, 501 (1997).
29. E. A. Boyle, *Paleoceanography* **3**, 471 (1988).
30. D. W. Lea, E. A. Boyle, *Nature* **347**, 269 (1990).
31. ———, *Paleoceanography* **5**, 719 (1990).
32. T.-H. Peng, W. A. Broecker, *Global Biogeochem. Cycles* **1**, 155 (1987).
33. W. S. Broecker, T.-H. Peng, *Nature* **356**, 587 (1992).
34. W. B. Curry, J. C. Duplessy, L. D. Labeyrie, N. J. Shackleton, *Paleoceanography* **3**, 317 (1988).
35. W. S. Broecker, T.-H. Peng, S. Trumbore, G. Bonani, W. Wolfli, *Global Biogeochem. Cycles* **4**, 103 (1990).
36. W. S. Broecker, E. Clark, *G*^{3} GC000151 (2001).
37. W. S. Broecker, J. Lynch-Stieglitz, E. Clark, I. Hajdas, G. Bonani, *G*^{3}, GC000177 (2001).
38. K. Matsumoto *et al.*, *Earth Planet. Sci. Lett.* **192**, 319 (2001).
39. We are indebted to P. Lohmann for steering us away from our size index method and toward his shell weight method. He also helped us get started and worked with us to intercalibrate our measurements with his. Samples for this study were supplied by Woods Hole Oceanographic Institute's W. Curry (Ceara Rise) and D. McCorkle (Ontong Java Plateau). We also acknowledge R. Lotti for access to the Lamont-Doherty Earth Observatory (LDEO) core collection. Support for this research was provided by National Science Foundation grant OCE-00-81809. This is LDEO contribution 6259.

6 July 2001; accepted 15 October 2001

Requirement of *Math1* for Secretory Cell Lineage Commitment in the Mouse Intestine

Qi Yang,[1] Nessan A. Bermingham,[2,4] Milton J. Finegold,[3] Huda Y. Zoghbi[1,2,4]*

The mouse small intestinal epithelium consists of four principal cell types deriving from one multipotent stem cell: enterocytes, goblet, enteroendocrine, and Paneth cells. Previous studies showed that *Math1*, a basic helix-loop-helix (bHLH) transcription factor, is expressed in the gut. We find that loss of *Math1* leads to depletion of goblet, enteroendocrine, and Paneth cells without affecting enterocytes. Colocalization of *Math1* with Ki-67 in some proliferating cells suggests that secretory cells (goblet, enteroendocrine, and Paneth cells) arise from a common progenitor that expresses *Math1*, whereas absorptive cells (enterocytes) arise from a progenitor that is *Math1*-independent. The continuous rapid renewal of these cells makes the intestinal epithelium a model system for the study of stem cell regeneration and lineage commitment.

The mouse gut begins developing at embryonic day 7.5 (E7.5). Invagination of the most anterior and posterior endoderm leads to the formation of the foregut and hindgut pockets, respectively, which extend toward each other and fuse to form the gut tube. By E15.5, the gut appears as a poorly differentiated, pseudostratified epithelium. From E15.5 to E19, nascent villi with a monolayer of epithelial cells develop in a duodenum-to-colon pattern. During the first two postnatal weeks, the intervillus epithelium, where proliferating and less differentiated cells reside, develops into the crypts of Lieberkühn. Stem cells in the intervillus epithelium (during embryogenesis) or crypts (in adulthood) give rise to four principle cell types: absorptive enterocytes or columnar cells, mucous-secreting goblet cells, regulatory peptide-secreting enteroendocrine cells in the large and small intestines, and antimicrobial peptide-secreting Paneth cells in the small intestine only. Enterocytic, goblet, and enteroendocrine cells continue to differentiate and mature while migrating up the villus, and are finally extruded into the lumen at the tip. This journey takes about 2 to 3 days. The Paneth cells migrate downward and reside at the base of the crypt for ~21 days before being cleared by phagocytosis (*1–3*).

The epithelial-mesenchymal interaction has been shown to be critical in the proximal-distal, crypt-villus patterning during gut development. A number of signaling molecules and transcription factors are involved in these processes (*4–7*). Previous studies have suggested that all four epithelial cell lineages originate from a common ancestor (*1–3, 8*), but the mechanisms that control the epithelial lineage differentiation are not well understood. T cell factor-4 (*Tcf4*) plays a role in the stem cell maintenance in the small intestine but does not induce epithelial cells to differentiate into enterocytes or goblet cells (*9*). Because *Math1* is expressed in the gut (*10*) and involved in cell fate determination in the nervous system (*11, 12*), we sought to determine its function during gut development.

We have two null alleles for *Math1*: *Math1*$^{-/-}$ (with the coding region replaced by *Hprt*) and *Math1*$^{\beta\text{-Gal}/\beta\text{-Gal}}$ (with the coding region replaced by the β-galactosidase gene, which is then expressed under the control of the *Math1* promoter) (*11*). *Math1* null mice die shortly after birth, but *Math1* heterozygous mice survive to adulthood and appear normal. We previously showed that *Math1/LacZ* expression faithfully mimics the endogenous gene expression (*11*). Here we used *Math1*$^{\beta\text{-Gal}/-}$ instead of *Math1*$^{\beta\text{-Gal}/\beta\text{-Gal}}$ null mice for X-gal staining experiments to ensure equal copy numbers of the *LacZ* gene in heterozygous and null animals.

Math1/LacZ expression within the gut is restricted to the intestinal epithelium starting at E16.5 and is sustained until adulthood (*13*). We detected no *Math1/LacZ* expression in the stomach, pancreas, or lung. In E18.5 heterozygous mice, *LacZ*-positive cells are sparsely scattered in the villi, the intervillus epithelium (Fig. 1A), and colonic crypts (Fig. 1C). In *Math1* null littermates, however, *LacZ*-expressing cells are clustered in the intervillus region of ileum (Fig. 1B) and at the bases of the colonic crypts (Fig. 1D). *Math1/LacZ* expression persists throughout duodenum, jejunum, ileum, and colon [Fig. 1, E and F, and Web fig. 1 (*14*)] in adult *Math1*$^{\beta\text{-Gal}/+}$ mice. In the villi, the scattered blue cells appear to have a goblet cell morphology (a spherical vacuole); at the base of the crypt, most apical granule-containing Paneth cells appear to be *LacZ*-positive. X-gal stained cells are also found in the mid-crypt region. *LacZ* expression in adult crypts suggests that *Math1* helps initiate cytodifferentiation of the epithelial cells.

We detected no *Math1/LacZ* expression

[1]Department of Pediatrics and Program in Developmental Biology, [2]Department of Molecular and Human Genetics, [3]Department of Pathology and [4]Howard Hughes Medical Institute, Baylor College of Medicine, Houston, TX 77030, USA.

*To whom correspondence should be addressed. E-mail: hzoghbi@bcm.tmc.edu